AAC Journals.ASM.org

Mass Spectrometry Imaging Reveals Heterogeneous Efavirenz Distribution within Putative HIV Reservoirs

Corbin G. Thompson,[a] Mark T. Bokhart,[b] Craig Sykes,[a] Lourdes Adamson,[c] Yuri Fedoriw,[d] Paul A. Luciw,[c] David C. Muddiman,[b] Angela D. M. Kashuba,[a] Elias P. Rosen[b]

Division of Pharmacotherapy and Experimental Therapeutics, University of North Carolina at Chapel Hill, Chapel Hill, North Carolina, USA[a]; W. M. Keck FTMS Laboratory for Human Health Research, Department of Chemistry, North Carolina State University, Raleigh, North Carolina, USA[b]; University of California, Davis, California, USA[c]; School of Medicine, University of North Carolina at Chapel Hill, Chapel Hill, North Carolina, USA[d]

Persistent HIV replication within active viral reservoirs may be caused by inadequate antiretroviral penetration. Here, we used mass spectrometry imaging with infrared matrix-assisted laser desorption–electrospray ionization to quantify the distribution of efavirenz within tissues from a macaque dosed orally to a steady state. Intratissue efavirenz distribution was heterogeneous, with the drug concentrating in the lamina propria of the colon, the primary follicles of lymph nodes, and the brain gray matter. These are the first imaging data of an antiretroviral drug in active viral reservoirs.

Human immunodeficiency virus (HIV) replication has been shown to persist in certain anatomic sites, known as active viral reservoirs, despite treatment with highly active antiretroviral (ARV) therapy (HAART) (1, 2). Understanding the factors that contribute to the formation and propagation of these active viral reservoirs is essential to the design of targeted therapies for HIV eradication. It has been suggested that subtherapeutic drug concentrations in certain tissues resulting from poor drug penetration may provide a favorable environment for reservoir formation and drug-resistant viral variants (3). Several groups, including our own, have assessed ARV penetration of tissues by directly measuring drug concentrations by liquid chromatography-mass spectrometry (LC-MS) of homogenized whole tissue (4) or isolated mononuclear cells (3, 5). Though these methods can provide useful quantitative data, they do not have the ability to spatially define the distribution of the drug within the tissue, as either the entire sample is consumed in the homogenization process or spatial information is lost during cellular isolation. This is a critical limitation of these methodologies, as our preliminary data have shown that ARV distribution across tissue is not uniform (6).

MS imaging (MSI) offers an alternative strategy for quantifying ARV distribution in tissues and cells that maintains the sensitivity and specificity of LC-MS while preserving the spatial distribution of analytes within tissue. Through stepwise interrogation of discrete sample locations, MSI simultaneously collects information that can be concatenated into images of multiple molecules and their respective metabolites. This attribute is an important advantage for the combinatorial nature of HAART and has already led to the implementation of MSI in the drug development process (7). One approach to MSI that is particularly well suited to the analysis of small molecules is infrared matrix-assisted laser desorption–electrospray ionization (IR-MALDESI) (8), which allows the detection of ARVs in human tissue, as we have previously demonstrated (9, 10).

Here, we used IR-MALDESI to characterize the ARV distribution in 11 nonhuman primate tissues implicated as viral reservoirs (11–14). Further, we quantified the variability in ARV exposure between tissues and compared this to LC-MS and immunohistochemistry (IHC) data, allowing for absolute quantification of observed ARV signal abundance and identification of the tissue compartments or cellular populations where a drug may be concentrating. These data are the first quantitative images of the ARV distribution in a macaque, an important species for studies of HIV/simian immunodeficiency virus (SIV) therapy, and show that MSI is a promising approach for evaluating ARV disposition in HIV reservoirs (15).

One healthy male rhesus macaque (*Macaca mulatta*) was given 7 daily oral doses of 200 mg of efavirenz (EFV). This dose of EFV equates to roughly 60 mg/kg and is consistent with standard treatment doses for SIV (16, 17). Prior to necropsy, blood plasma and cerebrospinal fluid were collected. The animal was euthanized by pentobarbital overdose 24 h after the final dose of EFV, and necropsy was performed by the pathology staff at the California National Primate Research Center. Tissue samples from the gastrointestinal (GI) tract (ileum, colon, rectum), central nervous system (CNS; cerebellum, basal ganglia), lymph nodes (axillary, iliac, mesenteric, inguinal), and spleen were snap-frozen on dry ice and stored at −80°C until analysis (18). Calibration of the IR-MALDESI response to EFV from the dosed tissue was conducted by MSI of tissues from nondosed ("blank") macaques (Bioreclamation IVT, Baltimore, MD), matching dosed tissue samples where possible, upon which a set of EFV standards were pipetted. Prior to imaging, 10-μm sections of each tissue (dosed and nondosed) were sliced and thaw mounted on a single glass microscope slide uniformly coated with internal standards and the tissue sections were spotted with 100 nl containing 0 to 5,000 pg of EFV before the sample slide was placed in the IR-MALDESI

Received 8 December 2014 **Returned for modification** 24 January 2015
Accepted 22 February 2015

Accepted manuscript posted online 2 March 2015

Citation Thompson CG, Bokhart MT, Sykes C, Adamson L, Fedoriw Y, Luciw PA, Muddiman DC, Kashuba ADM, Rosen EP. 2015. Mass spectrometry imaging reveals heterogeneous efavirenz distribution within putative HIV reservoirs. Antimicrob Agents Chemother 59:2944–2948. doi:10.1128/AAC.04952-14.

Address correspondence to Elias P. Rosen, erosen@ncsu.edu.

doi:10.1128/AAC.04952-14

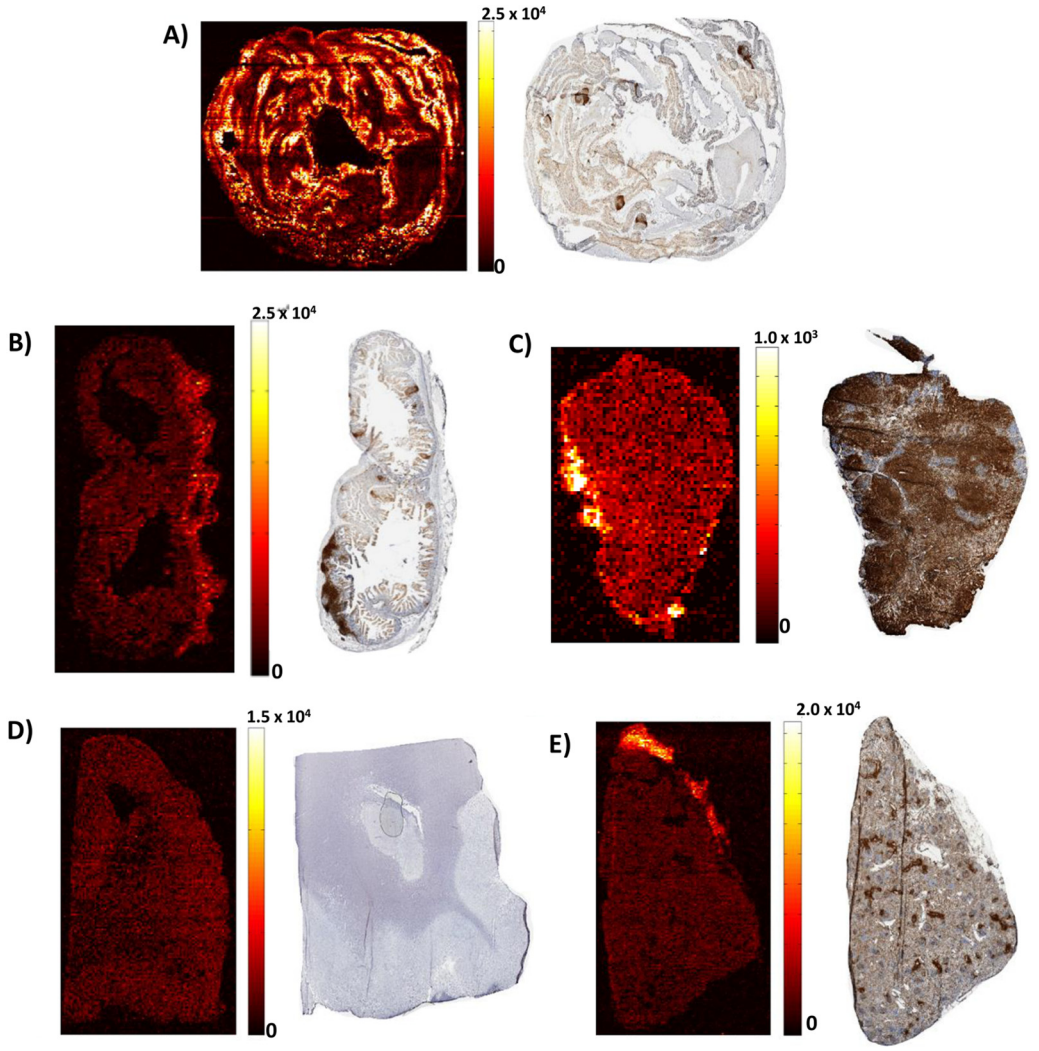

FIG 1 EFV distribution in macaque reservoir sites. Representative MSI images are shown on the left, with adjacent $CD3^+$ cell staining of serial colon (A), ileum (B), inguinal lymph node (C), cerebellum (D), and spleen (E) tissue slices. MSI signal intensity is shown next to each image on a concentration-dependent scale. The bottom of the scale (0) represents the presence of no EFV, while the top of the scale reflects the highest per-voxel EFV signal observed within each slice. Brighter colors represent higher EFV concentrations.

imaging source. Serial 10-μm sections were set aside for LC-MS/MS and IHC analyses.

The IR-MALDESI MSI approach for analysis of tissue samples has been described previously (8, 9). Briefly, tissue samples maintained at −10°C in the source chamber were ablated at a spot-to-spot distance of 100 μm by two pulses of an IR laser (IR-Opolette 2371; Opotek, Carlsbad, CA, USA) that resulted in the complete desorption of neutral molecules for a given volume element or voxel. The desorbed neutral molecules were then ionized by an orthogonal electrospray plume and sampled into a high-resolving-power Thermo Fisher Scientific Q Exactive (Bremen, Germany) mass spectrometer for synchronized analysis (9). To generate images from mass spectrometry data, raw data from each voxel were converted to the mzXML format with MSConvert software (19). These mzXML files were interrogated with MSiReader, a free software developed for processing of MSI data, from which measurements such as tissue surface area can be made and images of analyte distribution can be generated (20).

For LC-MS/MS analysis of EFV concentrations, serial 10-μm tissue sections were homogenized in 1 ml of 70:30 acetonitrile–1 mM ammonium phosphate (pH 7.4) with a Precellys 24 tissue homogenizer (Bertin Technologies, Montigny-le-Bretonneux, France). A Shimadzu high-performance liquid chromatography system was used for separation, and an AB SCIEX API 5000 mass spectrometer (AB SCIEX, Foster City, CA, USA) equipped with a turbo spray interface was used as the detector. The samples were analyzed with a set of calibration standards (0.02 to 20 ng) and quality control (QC) samples. The precision and accuracy of the calibration standards and QC samples were within the acceptable range of 15%. LC-MS/MS quantification of EFV in the homogenate of each tissue section was compared to the summed MSI response on a per-mass-of-tissue basis by using the MSI-derived tissue surface area, the known section thickness, and an assumed tissue density of 1.06 g/cm^3. MSI quantitation and LC-MS/MS analysis were performed by different individuals at separate institutions, and no data were shared before analyses were completed.

TABLE 1 Variability of EFV MSI responses within dosed macaque tissues

Tissue type	No. of ng/voxel[a]			DR (dB)[b]
	Maximum	Median	Minimum	
CNS				
Cerebellum	1.8E+04	5.0E+03	6.5E+02	14.5
Basal ganglion	1.8E+03	9.2E+02	4.8E+02	5.8
Lymph node				
Axillary	3.0E+04	4.2E+03	2.0E+03	11.8
Mesenteric	9.8E+03	2.6E+03	1.1E+03	9.5
Inguinal	2.7E+04	1.6E+03	8.1E+02	15.2
Iliac	4.0E+03	9.3E+02	3.4E+02	10.7
Spleen	4.2E+04	5.1E+03	1.4E+03	14.6
GI tract				
Ileum	1.4E+04	3.7E+03	2.5E+03	7.5
Colon	8.7E+06	1.4E+04	1.5E+03	37.6
Rectum	1.6E+06	1.2E+04	3.4E+03	26.8
Testis	2.7E+03	5.9E+02	3.7E+02	8.6

[a] The EFV concentration within each voxel across the entire tissue slice was quantified by using calibration standards.
[b] Dynamic range (DR), expressed in the logarithmic units decibels, was calculated as DR = $10\log_{10}$(maximum/minimum).

The LC-MS/MS data underwent QC by a designated individual not directly involved in this study to ensure accuracy.

To verify tissue quality and assess architecture for comparison with EFV distribution by MSI, serial sections of frozen tissue were sliced at a 10-μm thickness, thaw mounted on glass slides, and fixed in 100% ethanol for 10 min. After fixation, the tissues were stained with hematoxylin and eosin by standard histological techniques. IHC analysis of similarly prepared frozen tissue slices was performed with human primary antibodies for CD3 (clone LN10; Leica Biosystems, Buffalo Grove, IL), followed by staining with secondary antibodies. All staining was performed with the Leica Bond automated tissue stainer (Leica Biosystems).

MSI revealed heterogeneous intratissue EFV distribution into several anatomic sites. Figure 1 showcases these findings for representative tissues. When MSI images were compared with IHC staining, interesting spatial distributions were noted. For example, EFV was concentrated in the mucosa and lamina propria of the colon (Fig. 1A), which corresponds to a high $CD3^+$ cell density on IHC analysis. However, this distribution was not observed in the ileum (Fig. 1B). The inguinal lymph node showed EFV in some, but not all, primary follicles (Fig. 1C). EFV concentrated in the gray matter of the cerebellum (Fig. 1D) and showed a homogeneous distribution in the spleen, testes, and axillary lymph nodes (Fig. 1E). The heterogeneity of EFV distribution is quantified in Table 1 by the dynamic range of the MSI response (expressed in the base 10 logarithmic units decibels [dB]) in each tissue type that can be observed in the images in Fig. 1. The dynamic range of the EFV response was lower in tissues such as the basal ganglia and lymph nodes, reflecting a more homogeneous EFV distribution, whereas tissues such as the colon (37.6 dB) and rectum (26.8 dB) had much larger differences between minimum and maximum concentrations that suggest greater biological differences in drug uptake.

Intertissue EFV quantitation is summarized in Table 2. LC-MS/MS analysis demonstrated a 20-fold variability in total tissue EFV exposure, with concentrations ranging from 1.2 μg/g in the testes to 20.8 μg/g in the colon. A similar trend was observed in the MSI quantification, though agreement varied between tissue types. EFV concentrations determined by MSI and LC-MS/MS were found to be in agreement (<30% difference) for half of the tissues after correction for tissue size. In tissues such as the lymph nodes, concentrations varied by as little as 8%. Tissues of the GI tract demonstrated less agreement between techniques, with variations of up to −70%. Table 2 also compares EFV exposures in

TABLE 2 Comparison of EFV quantitations in macaque tissues by MSI and LC-MS/MS

Tissue type	LC-MS/MS		MSI		Difference[c] (%)
	Concn (μg/g tissue)[a]	Log increase over plasma or CSF[b]	Concn (μg/g tissue)	Log increase over plasma or CSF[b]	
CNS					
Cerebellum	6.86	7.6	3.09	6.8	−54.89
Basal ganglion	2.01	6.4	1.67	6.2	−16.80
Lymph node					
Axillary	3.91	2.0	3.33	1.8	−14.91
Mesenteric	3.82	2.0	3.12	1.8	−18.48
Inguinal	4.80	2.2	2.86	1.7	−40.38
Iliac	2.82	1.7	3.06	1.7	8.40
Spleen	5.01	2.2	3.61	1.9	−27.83
GI tract					
Ileum	8.41	2.7	3.20	1.8	−61.94
Colon	20.77	3.6	6.12	2.4	−70.54
Rectum	20.69	3.6	8.22	2.7	−60.26
Testis	1.22	0.8	2.91	1.7	138.94

[a] On day 8, the concentrations in plasma and CSF were 541 and 3.30 ng/ml, respectively, as measured by LC-MS/MS.
[b] To compare tissue drug concentrations to plasma or CSF drug concentrations, tissue drug concentrations in μg/g were converted to ng/ml, assuming a tissue density of approximately 1 g/ml, and then divided by the plasma or CSF drug concentration and converted to log units.
[c] The percent difference between methods was calculated by subtracting LC-MS/MS concentrations from MSI concentrations, dividing by the LC-MS/MS concentration, and multiplying by 100.

tissue and plasma. EFV achieved high exposure in the CNS, where tissue drug concentrations were 6.8 to 7.6 log units higher than in the CSF. EFV exposure was consistent among the lymph nodes, with 1.7- to 2.2-log increases over plasma observed. In the GI tract, EFV exposure was 3.6 log units higher than in plasma in the colon and rectum and 2.7 log units higher in the ileum.

The persistence of HIV replication within anatomic reservoirs necessitates the use of tissue pharmacology to inform the design of effective treatment strategies. This requires knowledge of tissue penetration to sites of action, as underscored by recent findings that the 50 to 90% reduction of the EFV concentration in mononuclear cells isolated from reservoir tissues relative to that in peripheral blood mononuclear cells was associated with persistent viral replication in these tissues (3). This finding, in combination with the fact that EFV receives widespread clinical use as a component of Atripla (a fixed-dose combination of tenofovir, emtricitabine, and EFV dosed once daily) and is frequently included in HIV treatment and cure research regimens for macaques, led us to choose EFV for our evaluations.

The observed ARV drug distribution within these putative viral reservoirs reveals important information regarding tissue pharmacology that can inform treatment strategy. The heterogeneous penetration of the lymphoid follicles by EFV suggests that further quantification of effective drug exposure in these tissues is required. Conversely, the abundance of EFV signal in the $CD3^+$ cell populations of the gut is evidence that adequate EFV concentrations are likely reached in this compartment. Both of these findings are consistent with previous studies that have examined tissue EFV concentrations by LC-MS (5). The EFV distributions observed here would not have been possible with traditional LC-MS of tissue homogenates or isolated mononuclear cells; the heterogeneity of EFV distribution within tissue slices as measured by the dynamic range of response (Table 1) is only measurable by MSI. Moreover, our MSI analysis provides evidence that the use of plasma or CSF as a surrogate for tissue drug concentrations may be inappropriate without detailed quantification of these relationships. The higher CNS tissue EFV concentrations than CSF EFV concentrations (Table 2) and the concentration of EFV within the gray matter of the cerebellum (Fig. 1) agree with brain microdialysis data showing that CNS drug concentrations are higher than CSF drug concentrations (21, 22).

The variability in the extent of EFV distribution between tissue types suggests that biological processes, more than the cellular populations present, drive the movement of EFV into tissues. The nonhomogeneous distribution of EFV in tissues such as the colon may be attributable to the physicochemical properties of EFV or to active transport mechanisms. Our previous work identifying variables affecting ARV exposure in the female genital tract (another putative viral reservoir) found that the efflux transporters MRP1 and MRP4 were associated with ARV penetration of this compartment (23). While EFV is not a known substrate of these transporters, other drug transporters such as MDR1 or BCRP may affect its disposition and explain the areas of EFV concentration seen here (24, 25).

There are several limitations of this analysis that should be addressed, the most important of which is our limited sample size. As this study was conducted with a single animal, the variability in tissue drug distribution between animals remains unknown and remains to be evaluated. Further, the assessment of EFV distribution shown in Fig. 1 is based on individual slices of tissue under steady-state conditions. Repeated sectioning may reveal additional biological variability. Although EFV has a long plasma half-life and a relatively flat blood plasma concentration-versus-time curve, EFV exposure over the dosing interval could not be determined because sampling was performed only at the end of the dosing interval. Additionally, we were unable to determine the relationship between drug and viral dynamics in this uninfected animal, though we selected tissues with previous evidence supporting persistent HIV infection (11–14). Finally, only CD3 was used to correlate IHC analysis with drug distribution. Though visualization of the overall T cell compartment is informative, future work will relate ARV localization to $CD4^+$ T cell distribution, as these cells are the most relevant for HIV infection.

This is the first study to apply MSI to ARV distribution in potential tissue reservoirs of HIV infection. Using IR-MALDESI, we have confirmed that ARV tissue distribution is heterogeneous and that the distribution of a single ARV can vary greatly between tissues within an individual. By comparison to the gold standard of tissue quantification, LC-MS/MS, our analysis confirms the importance of MSI for drug quantification. Future work will address the existing limitations of our approach. For MSI, this will entail a systematic exploration of factors, such as matrix effects or electrospray ionization capacity, that may influence the quantitative agreement with LC-MS for different tissue types and drug exposures. IR-MALDESI is sensitive to a wide variety of endogenous lipids (the profiles of which vary between tissue types) that are ablated and analyzed simultaneously with EFV. Any suppression of the EFV response as a result of tissue-specific ablation and ionization conditions is intended to be taken into account by performing EFV calibrations with matching or closely related blank tissue types and evaluating the IR-MALDESI response to an internal standard. However, a more thorough investigation of these effects must be undertaken to improve analytical agreement. Additionally, lower limits of detection of all ARVs and their active metabolites within a drug regimen must be attained in order to link tissue drug exposure and suppression of viral replication. We will also evaluate ARV distribution in SIV/HIV-infected samples to determine the effect of ARV disposition on viral expression. Despite these limitations, these data show that MSI is a critical tool for the disposition of ARVs within putative active HIV reservoirs, which is an important step toward understanding how to eradicate HIV infection.

ACKNOWLEDGMENTS

This work was supported by NIH grants R01AI111891 (E.P.R., C.G.T., C.S., Y.F., P.A.L., D.C.M., and A.D.M.K.), R01GM087964 (E.P.R., M.T.B., and D.C.M.), and U01AI095031, UNC Center for AIDS Research grant P30AI050410 (C.G.T., C.S., Y.F., A.D.M.K., and E.P.R.), and Collaboratory of AIDS Researchers for Eradication (CARE) grant U19AI096113.

We also acknowledge additional support from GlaxoSmithKline, the William R. Kenan, Jr. Fund for Engineering, Technology, and Science, and the W. M. Keck Foundation (E.P.R., M.T.B., and D.C.M.).

REFERENCES

1. **Palmer S, Josefsson L, Coffin JM.** 2011. HIV reservoirs and the possibility of a cure for HIV infection. J Intern Med **270:**550–560. doi:http://dx.doi.org/10.1111/j.1365-2796.2011.02457.x.
2. **Chun T-W, Nickle DC, Justement JS, Meyers JH, Roby G, Hallahn CW, Kottilil S, Moir S, Mican JM, Mullins JI, Ward DJ, Kovacs JA, Mannon PJ, Fauci AS.** 2008. Persistence of HIV in gut-associated lymphoid tissue

despite long-term antiretroviral therapy. J Infect Dis **197:**714–720. http://dx.doi.org/10.1086/527324.
3. **Fletcher CV, Staskus K, Wietgrefe SW, Rothenberger M, Reilly C, Chipman JF, Beilman GJ, Khoruts A, Thorkelson A, Schmidt TE, Anderson J, Perkey K, Stevenson M, Perelson AS, Douek DC, Haase AT, Schacker TW.** 2014. Persistent HIV-1 replication is associated with lower antiretroviral drug concentrations in lymphatic tissues. Proc Natl Acad Sci U S A **111:**2307–2312. http://dx.doi.org/10.1073/pnas.1318249111.
4. **Dumond JB, Yeh RF, Patterson KB, Corbett AH, Jung BH, Rezk NL, Bridges AS, Steward PW, Cohen MS, Kashuba AD.** 2007. Antiretroviral drug exposure in the female genital tract: implications for oral pre- and post-exposure prophylaxis. AIDS **21:**1899–1907. http://dx.doi.org/10.1097/QAD.0b013e328270385a.
5. **Podany AT, Winchester LC, Robbins BL, Fletcher CV.** 2014. Quantification of cell-associated atazanavir, darunavir, lopinavir, ritonavir, and efavirenz concentrations in human mononuclear cell extracts. Antimicrob Agents Chemother **58:**2866–2870. http://dx.doi.org/10.1128/AAC.02551-13.
6. **Thompson CG, Rosen E, Sykes C, Fedoriw Y, Luciw PA, Muddiman DC, Kashuba AD.** 2014. Characterizing antiretroviral distribution within active viral reservoirs using mass spectrometry imaging, abstr p_09, p 36–37. Abstract Book 15th International Workshop on Clinical Pharmacology of HIV & Hepatitis Therapy, Washington, DC. http://regist2.virology-education.com/abstractbook/2014_4.pdf.
7. **Prideaux B, Stoeckli M.** 2012. Mass spectrometry imaging for drug distribution studies. J Proteomics **75:**4999–5013. http://dx.doi.org/10.1016/j.jprot.2012.07.028.
8. **Robichaud G, Barry JA, Garrard KP, Muddiman DC.** 2013. Infrared matrix-assisted laser desorption electrospray ionization (IR-MALDESI) imaging source couple to a FT-ICR mass spectrometer. J Am Soc Mass Spectrom **24:**92–100. http://dx.doi.org/10.1007/s13361-012-0505-9.
9. **Barry JA, Robichaud G, Bokhart MT, Thompson CG, Sykes C, Kashuba AD, Muddiman DC.** 2014. Mapping antiretroviral drugs in tissue by IR-MALDESI MSI coupled to the Q Exactive and comparison with LC-MS/MS SRM assay. J Am Soc Mass Spectrom **25:**2038–2047. http://dx.doi.org/10.1007/s13361-014-0884-1.
10. **Bokhart MT, Rosen E, Thompson C, Sykes C, Kashuba AD, Muddiman DC.** 16 October 2014. Quantitative mass spectrometry imaging of emtricitabine in cervical tissue model using infrared matrix-assisted laser desorption electrospray ionization. Anal Bioanal Chem http://dx.doi.org/10.1007/s00216-014-8220-y.
11. **Gratton S, Cheynier R, Dumaurier M-J, Oksenhendler E, Wain-Hobson S.** 2000. Highly restricted spread of HIV-1 and multiply infected cells within splenic germinal centers. Proc Natl Acad Sci U S A **97:**14566–14571. http://dx.doi.org/10.1073/pnas.97.26.14566.
12. **Burton GF, Keele BF, Estes JD, Thacker TC, Gartner S.** 2002. Follicular dendritic cell contributions to HIV pathogenesis. Immunology **14:**275–284. http://dx.doi.org/10.1016/S1044-5323(02)00060-X.
13. **Avettand-Fenoel V, Hocqueloux L, Muller-Trutwin M, Prazuck T, Melard A, Chaix ML, Agoute E, Michau C, Rouzioux C.** 2011. Greater diversity of HIV DNA variants in the rectum compared to variants in the blood in patients without HAART. J Med Virol **83:**1499–1507. http://dx.doi.org/10.1002/jmv.22132.
14. **Zink MC, Clements JE.** 2002. A novel simian immunodeficiency virus model that provides insight into mechanisms of human immunodeficiency virus central nervous system disease. J Neurovirol **8**(Suppl 2)**:**S42–S48. http://dx.doi.org/10.1080/13550280290101076.
15. **Van Rompay KK.** 2012. The use of nonhuman primate models of HIV infection for the evaluation of antiviral strategies. AIDS Res Hum Retroviruses **28:**16–35. http://dx.doi.org/10.1089/aid.2011.0234.
16. **North TW, Van Rompay KK, Higgins J, Matthews TB, Wadford DA, Pedersen NC, Schinazi RF.** 2005. Suppression of virus load by highly active antiretroviral therapy in rhesus macaques infected with a recombinant simian immunodeficiency virus containing reverse transcriptase from human immunodeficiency virus type 1. J Virol **79:**7349–7354. http://dx.doi.org/10.1128/JVI.79.12.7349-7354.2005.
17. **Hofman MJ, Higgins J, Matthews TB, Pedersen NC, Tan C, Schinazi RF, North TW.** 2004. Efavirenz therapy in rhesus macaques infected with a chimera of simian immunodeficiency virus containing reverse transcriptase from human immunodeficiency virus type 1. Antimicrob Agents Chemother **48:**3483–3490. http://dx.doi.org/10.1128/AAC.48.9.3483-3490.2004.
18. **North TW, Higgins J, Deere JD, Hayes TL, Villalobos A, Adamson L, Schacklett BL, Schinazi RF, Luciw PA.** 2010. Viral sanctuaries during highly active antiretroviral therapy in a nonhuman primate model for AIDS. J Virol **84:**2913–2922. http://dx.doi.org/10.1128/JVI.02356-09.
19. **Kessner D, Chambers M, Burke R, Agus D, Mallick P.** 2008. ProteoWizard: open source software for rapid proteomics tools development. Bioinformatics **24:**2534–2536. http://dx.doi.org/10.1093/bioinformatics/btn323.
20. **Robichaud G, Garrard KP, Barry JA, Muddiman DC.** 2013. MSiReader: an open-source interface to view and analyze high resolving power MS imaging files on Matlab platform. J Am Soc Mass Spectrom **24:**718–721. http://dx.doi.org/10.1007/s13361-013-0607-z.
21. **Liu X, Natta Van K, Yeo H, Vilenski O, Weller PE, Worboys PD, Monshouwer M.** 2009. Unbound drug concentration in brain homogenate and cerebral spinal fluid at steady state as a surrogate for unbound concentration in brain interstitial fluid. Drug Metab Dispos **37:**787–793. http://dx.doi.org/10.1124/dmd.108.024125.
22. **de Lange E, Danhof M.** 2002. Cerebrospinal fluid pharmacokinetics to predict brain target concentrations in the clinical setting: implications of the barriers between blood and brain. Clin Pharmacokinet **41:**691–703. http://dx.doi.org/10.2165/00003088-200241100-00001.
23. **Thompson CG, Sedykh A, Nicol MR, Muratov E, Fourches D, Tropsha A, Kashuba AD.** 2014. Cheminformatics analysis to identify predictors. AIDS Res Hum Retroviruses **30:**1058–1064. http://dx.doi.org/10.1089/aid.2013.0254.
24. **Peroni RN, Di Gennaro SS, Hocht C, Chiappetta DA, Rubio MC, Sosnik A, Bramuglia GF.** 2011. Efavirenz is a substrate and in turn modulates the expression of the efflux transporter ABCG2/BCRP in the gastrointestinal tract of the rat. Biochem Pharmacol **82:**1227–1233. http://dx.doi.org/10.1016/j.bcp.2011.07.081.
25. **Fellay J, Marzolini C, Meaden ER, Back DJ, Buclin T, Chave JP, Decosterd LA, Furrer J, Opravil M, Pantaleo G, Retelka D, Ruiz L, Schinkel AH, Vernazza P, Eap CB, Telenti A.** 2002. Response to antiretroviral treatment in HIV-1-infected individuals with allelic variants of the multidrug resistance transporter 1: a pharmacogenetics study. Lancet **359:**30–36. http://dx.doi.org/10.1016/S0140-6736(02)07276-8.